

Reproduction of AdEx dynamics on neuromorphic hardware through data embedding and simulation-based inference

Jakob Huhle*, Jakob Kaiser*[†], Eric Müller* and Johannes Schemmel*

*Kirchhoff Institute for Physics, Heidelberg University, Germany

[†]Jakob.Kaiser@kip.uni-heidelberg.de

Abstract—The development of mechanistic models of physical systems is essential for understanding their behavior and formulating predictions that can be validated experimentally. Calibration of these models, especially for complex systems, requires automated optimization methods due to the impracticality of manual parameter tuning. In this study, we use an autoencoder to automatically extract relevant features from the membrane trace of a complex neuron model emulated on the BrainScaleS-2 neuromorphic system, and subsequently leverage sequential neural posterior estimation (SNPE), a simulation-based inference algorithm, to approximate the posterior distribution of neuron parameters.

Our results demonstrate that the autoencoder is able to extract essential features from the observed membrane traces, with which the SNPE algorithm is able to find an approximation of the posterior distribution. This suggests that the combination of an autoencoder with the SNPE algorithm is a promising optimization method for complex systems.

Index Terms—neuromorphic computing, simulation-based inference, AdEx, autoencoder

I. INTRODUCTION

In science, researchers endeavor to develop mechanistic models for physical systems. Subsequently, these models can be utilized to comprehend the behavior of the system and to formulate predictions that can be subjected to experimental verification. Once a model candidate has been identified, the model parameters must be calibrated to ensure that the model can reproduce the observed behavior of the system.

In the case of complex models, manual tuning of the parameters is not a viable option; instead, automated optimization methods are required [1]. Genetic algorithms have been demonstrated to be an effective approach for identifying parameters in complex models within the field of neuroscience [1]–[3]. Gradient-based optimization methods are capable of directed optimization, which makes them potentially more efficient for finding suitable model parameters [4]. Simulation-based inference (SBI) methods can be employed to approximate the posterior distribution of model parameters, thereby providing additional insight into the sensitivity and correlation of the parameters [5]–[9].

In previous applications of the sequential neural posterior estimation (SNPE) algorithm, an SBI algorithm, to neuroscientific problems, experiments relied on handcrafted features which were extracted from the recordings of neural traces [8], [10]. In the present study, we utilize an autoencoder to extract relevant

features from the membrane trace of a complex neuron model emulated on the BrainScaleS-2 (BSS-2) neuromorphic system [10], [11] and subsequently employ the SNPE algorithm to approximate the parameters of the neuron model. It is our hope that the automatic feature extraction facilitated by autoencoders will prove instrumental in enabling the application of SBI methods to more complex problems, thereby alleviating the need for handcrafted features.

A. The BrainScaleS-2 System

BSS-2 is a mixed-signal neuromorphic system; while synapse and neuron dynamics are emulated in analog circuits, spike communication and configuration is handled digitally [11], [12]. The system provides 512 analog neuron circuits which emulate the dynamics of the adaptive exponential integrate-and-fire (AdEx) [13] neuron model in continuous time [12]:

$$C_m \frac{dV_m(t)}{dt} = g_L \cdot (V_L - V_m(t)) + g_L \Delta_T \exp\left(\frac{V_m(t) - V_T}{\Delta_T}\right) + I_{\text{syn}}(t) + I(t) - w(t), \quad (1)$$

where V_m is the membrane potential, C_m the membrane capacitance, V_L the leak potential, g_L the leak conductance, Δ_T the threshold slope factor and V_T the effective threshold potential.

$I_{\text{syn}}(t)$ describes the synaptic current and will not be used in this study; $I(t)$ is an arbitrary current injected on the membrane. $w(t)$ represents an adaptation current with the following dynamics

$$\tau_w \frac{dw(t)}{dt} = a (V_m(t) - V_L) - w(t), \quad (2)$$

here a is the subthreshold adaptation and $\tau_w = \frac{C_w}{g_{\tau_w}}$ the adaptation time constant which is determined by the ratio of the capacitance C_w and the conductance g_{τ_w} .

As soon as the membrane potential V_m reaches the threshold potential V_{th} , the membrane potential is set to the reset potential V_r and the adaptation current is increased by the spike-triggered adaptation b : $w \rightarrow w + b$. The membrane potential V_m is kept at the reset potential V_r during the refractory period τ_{ref} ; afterwards it evolves according to eq. (1) again.

The circuits are implemented in 65 nm complementary metal-oxide semiconductor (CMOS) technology. Compared to the biological time domain, the neuron dynamics evolve in accelerated time with a tunable speed; in this study, we choose a speed-up factor of 1000.

The parameters of each neuron can be configured individually using a capacitor-based memory array [14]; the array is configured using digital 10 bit values and provides analog currents and voltages which control the behavior of the neuron¹.

B. Simulation-based Inference

SBI offers the possibility to approximate the posterior distribution of model parameters even if the likelihood is not tractable, i.e. it can not be calculated or is too expensive to calculate. More precisely, given a model $\mathcal{M} : \Theta \rightarrow X$ which is configured by the parameters $\theta \in \Theta$ and creates observations $x \in X$, SBI can be used to approximate the posterior distribution $p(\theta | x^*)$ for a given target observation $x^* \in X$. In this manuscript we will use the SNPE algorithm [6], [7], [15] to approximate the posterior distribution of AdEx parameters. The algorithm takes a mechanistic model \mathcal{M} , a prior distribution of the model parameters $p(\theta)$ and a target observation x^* as an input.

As a first step, random parameters $\theta' \sim p(\theta)$ are drawn from the prior. These parameters are injected in the model \mathcal{M} to produce observations $\{x'\}_i$. Therefore, we implicitly sample from the likelihood $x' \sim p(x | \theta')$.

The random parameters and observations $\{\theta', x'\}_i$ are then used to train a neural density estimator (NDE)² which approximates the posterior distribution $p(\theta | x)$. During training the negative log-likelihood of the posterior density estimate of the drawn samples $\{\theta', x'\}_i$ is minimized and the NDE learns to approximate the posterior distribution $p(\theta | x)$ for any observation x .

This posterior can then be used to draw additional samples for a given target observation x^* and to train the NDE again to improve the approximation of the posterior for the given observation³. This step can be repeated several times to further improve the approximation. For further details on the SNPE algorithm and its applications see [6]–[8], [10].

C. Autoencoder

High-dimensional data often contains redundant or irrelevant information for the task at hand. In deep learning, this can necessitate higher model complexity, prolong training times, and increase the risk of overfitting, which leads to worse performance in generalization on new, unseen data. Therefore, dimensionality reduction techniques can be employed to learn a lower-dimensional representation of the original data.

¹The last value is reserved such that the parameters are adjustable in a range from 0 to 1022.

²NDEs are flexible sets of probability distributions which are configured by neural networks; we will use a masked autoregressive flow (MAF) [8], [16], [17] as an NDE.

³After this step the posterior approximation is no longer amortized, i.e. it cannot be used to infer parameters for any observation x but only for the target observation x^* .

An autoencoder is an unsupervised deep learning model that can be leveraged for such a dimensionality reduction task. It consists of two neural networks: an encoder and a decoder. The encoder transforms the data into a lower-dimensional feature space, referred to as the latent space. Conversely, the decoder then maps the features from the latent space back to the original input space, aiming to recover the original input. The autoencoder is thus trained by minimizing a distance metric, quantifying the difference between the original data and its reconstruction. Once the model is successfully trained, the encoder can be used independently to obtain a lower-dimensional representation for each data sample.

For more information on autoencoders, see [18], [19].

II. METHODS

We first introduce the experimental routine with which we will record the behavior of an AdEx neuron on BSS-2. Next, we explain how we create a dataset which will then be used to train an autoencoder. Finally, we employ that trained autoencoder to extract relevant features from the experiment observation and utilize the SNPE algorithm to approximate the posterior distribution of model parameters.

A. Experimental Setup

Similar to [20], we investigate the behavior of a single AdEx neuron when stimulated with a step current $I(t)$, compare eq. (1). We emulate the dynamics on the BSS-2 system and record the membrane potential V_m for 1 ms^4 after the step current was enabled. The recorded membrane trace is then down sampled to 10 000 data points to reduce memory consumption and computational cost in subsequent steps. We manually chose parameters which will be used to create a target observation x^* . Four of these parameters will later be altered to create a dataset and to see if the SNPE algorithm is able to find an approximation of their posterior distribution: the adaptation parameters a , b and g_{τ_w} as well as the reset potential V_r , compare section I-A.

The BSS-2 operating system was used for experiment definition as well control [21] and experiments are written in the PyNN domain specific language [22].

B. Dataset

In order to train the autoencoder, we create a dataset with traces recorded from the hardware. To create a diverse set of samples, we will draw random values from a uniform distribution which covers the whole configuration range of the BSS-2 system for the four parameters we want to infer with the SNPE algorithm, see section II-A.

We draw a total of 200 000 parameterizations, emulate the model on BSS-2 and store the recorded membrane traces in a dataset.

⁴Due to the 1000-fold speed up of the BSS-2 system, this corresponds to 1 s in biological time.

Table I
ARCHITECTURE OF THE AUTOENCODER – THE AUTOENCODER IS BASED ON [19] AND RECEIVES AN INPUT OF SHAPE (1, 1024). THE BATCH DIMENSION OF 32 IS OMITTED FOR READABILITY.

Layer	Activation	Output Shape	Kernel Shape	Trainable Parameters
<i>Encoder</i>				
Conv 1D	ReLU	(32, 1024)	5	192
BatchNorm 1D	–	(32, 1024)		64
MaxPool 1D	–	(32, 512)	2	
Conv 1D	ReLU	(16, 512)	3	1552
BatchNorm 1D	–	(16, 512)		32
MaxPool 1D	–	(16, 256)	2	
Conv 1D	ReLU	(64, 256)	11	11 328
MaxPool 1D	–	(64, 128)	2	
Conv 1D	ReLU	(128, 128)	13	106 624
MaxPool 1D	–	(128, 64)	2	
Conv 1D	ReLU	(1, 64)	3	385
MaxPool 1D	–	(1, 32)	2	
<i>Decoder</i>				
Conv 1D	ReLU	(128, 32)	3	512
Upsample	–	(128, 64)		
Conv 1D	ReLU	(64, 64)	13	106 560
Upsample	–	(64, 128)		
Conv 1D	ReLU	(16, 128)	11	11 280
Upsample	–	(16, 256)		
Conv 1D	ReLU	(32, 256)	3	1568
Upsample	–	(32, 512)		
Conv 1D	–	(1, 512)	5	161
Upsample	–	(1, 1024)		
Total				240 258

C. Data Embedding

We use a convolutional autoencoder based on [19] to compress our high-dimensional observation. The model consist of several one-dimensional convolutions, ReLU activation functions, batch normalizations and max pooling layers, see table I. The input is compressed from 1024 data points to 32 data points.

Before feeding the data in our network, we preprocess it. First, we further down sample the recorded membrane traces from 10 000 to 1024 data points such that they fit the input layer of our network. Next, we normalize the recorded membrane voltages V_m to be in the range from 0 to 1. Since we use an analog-to-digital converter (ADC) with 10 bit resolution to sample the membrane voltage, this can be archived by dividing all values by 1023^5 .

The dataset is split into training, validation and test set with a ratio of 8/1/1. Afterwards, the training set is divided in batches of size 32 and the autoencoder is trained for 150 epochs. The mean-squared-error between the original trace and the reconstructed trace was used as a loss function. In each epoch, we record the loss of each batch on the training as well as the validation set. After each epoch, we save the model parameters if the validation loss has decreased.

We used the Adam optimizer [23] for updating the weights of the autoencoder. During a warm-up phase, the learning rate

⁵The ADC is configured such that the maximum of the readout range is never reached.

was linearly increased from 1×10^{-8} to the base learning rate of 1×10^{-4} in the first 2000 batches. After epoch 70, the learning rate was decreased exponentially with a factor of 0.94.

The model and training are implemented in the PyTorch library [24].

D. Simulation-based Inference

After successful training of the autoencoder, we use it in conjunction with an NDE to approximate the posterior of the parameters we altered during the generation of the dataset. The experimental observation is fed into the encoder section of the trained autoencoder, while the NDE receives the output from its latent space. We use a MAF with five transformations – each transformation is made up of two blocks with 50 hidden units per block – as an NDE; this NDE has been extensively used in previous publications [8], [10], [25].

Similarly to the generation of the dataset, we use uniform priors over the whole parameter range as an input to the SNPE algorithm. We train the NDE for 20 rounds with 1000 samples in each round. The pre-trained encoder is used to reduce the dimensionality of the observed data. During the training of the NDE, the encoder is further retrained in parallel to improve inference performance. This transfer learning approach for the encoder is motivated by the idea that the optimal features for reconstruction may not necessarily be the most suitable for parameter inference. At the same time, it allows for faster convergence compared to training from scratch.

We used the implementation of the `sbi` Python package [26] for the SNPE algorithm. This package supports the parallel training of the autoencoder and the NDE.

III. RESULTS

In the following, we will first present the generated dataset. Next, we train an autoencoder using this dataset and evaluate how well the reconstruction agrees with the original traces. Finally, we use the encoder part of the trained autoencoder to reduce the dimensionality of our observations and train a NDE using the SNPE algorithm.

A. Dataset

Figure 1 displays examples of traces in the dataset. In most cases, the neuron fires over the whole displayed range.

The variation in the reset potential V_r is most visible in the given example traces. In cases where the reset voltage is high, the membrane potential remains at high values and spikes are not clearly visible. In one case, a clear adaptation is visible: the inter-spike interval increases from spike to spike and the neuron stops firing after the third spike.

B. Data Embedding

We trained the autoencoder introduced in section II-C for 150 epochs. The training as well as the test loss decrease during training and start to saturate at the end of the training, fig. 2, indicating that the chosen number of epochs is sufficient. The difference between the two losses remains small, indicating

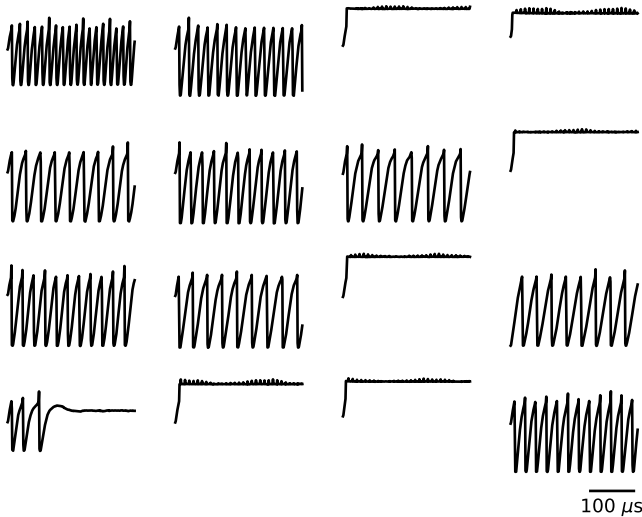


Figure 1. **Random samples drawn from the dataset.** – For visualization, only the first 300 μs are displayed; the traces are recorded for 1 ms. Due to the finite sampling frequency of the ADC and the interpolation of the recorded traces, the potentials at spike time are not identical. When the reset potential V_r is high, the membrane voltage remains at high levels.

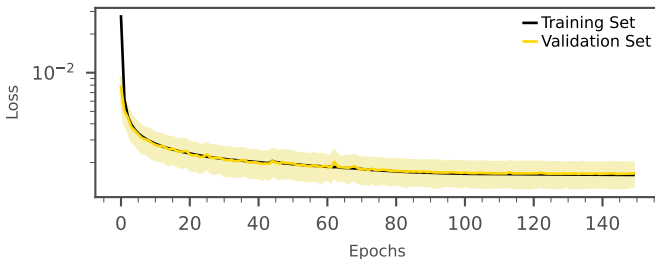


Figure 2. **Training of the autoencoder** – Mean test and validation loss during training as well as one standard deviation of the validation loss. Both losses decrease continuously over the course of the training.

that the model does not tend to overfit. We recorded the lowest validation loss after 140 epochs and will use this model for all future evaluations. At this point, the validation loss (0.001 63) is close to the test loss (0.001 64); further suggesting that our model does not overfit.

In fig. 3, we drew random samples from the test set and fed them into the trained autoencoder. Overall, the reconstructions follow the original samples closely. The reconstructions of periodic membrane traces are slightly better than of traces for which the inter-spike interval changes due to adaptation. On a fast time scale, the reconstructions show fluctuations which are not present in the original trace.

C. Simulation-based Inference

After estimating the posterior with the SNPE algorithm, we drew samples from it, fig. 4. The samples are closely scattered around the parameters which were used to create the target observation.

The distribution of parameters is narrowest for the reset potential V_r and the conductance g_{τ_w} controlling the adaptation

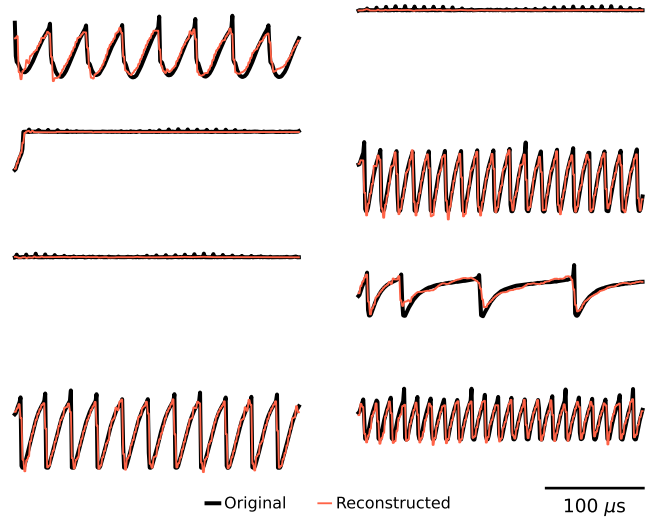


Figure 3. **Reconstructions of the autoencoder** – Randomly drawn voltage traces from the test set and their reconstructions by the trained autoencoder. Traces are only displayed for 300 μs to aid visual comparison. The reconstructions (red) follow the original traces (black) closely on a long time scale. However, unlike the original traces, they show some high frequency fluctuations.

time constant. This indicates that the observations are more sensitive to these two parameters than to the subthreshold adaptation a and the spike-triggered adaptation b .

Most of the parameters seem uncorrelated. Only for the spike-triggered adaptation b and the conductance g_{τ_w} a negative correlation can be observed: smaller values in g_{τ_w} can be compensated by higher values in b . Based on the design of the circuit, a dependency of the strength of the adaptation current w on the adaptation time constant τ_w is expected [12]. This effect can be compensated by adjusting the spike-triggered adaptation b .

In order to get an impression how well parameters drawn from the posterior distribution reproduce the target observation, we drew random values from the posterior, fig. 4, and emulated the neuron behavior with them, fig. 5. The recorded membrane traces match the target trace closely until the second spike. Afterwards, the traces start to diverge from the target observation. The divergence can to some extent be attributed to temporal noise in the analog core on BSS-2. As a comparison, fig. 5 also shows membrane recordings for the same parameters with which the target observation was recorded. Here, the traces also start to diverge after the second spike.

In comparison to the trial-to-trial variations, the variations in the traces recorded for different parameters drawn from the posterior seem more pronounced. Nevertheless, given the diversity seen in the traces of the dataset, fig. 1, the approximated posterior seems to yield parameters which closely resemble the given target observation.

IV. DISCUSSION

In this study, we demonstrated that the sequential neural posterior estimation (SNPE) algorithm can be successfully

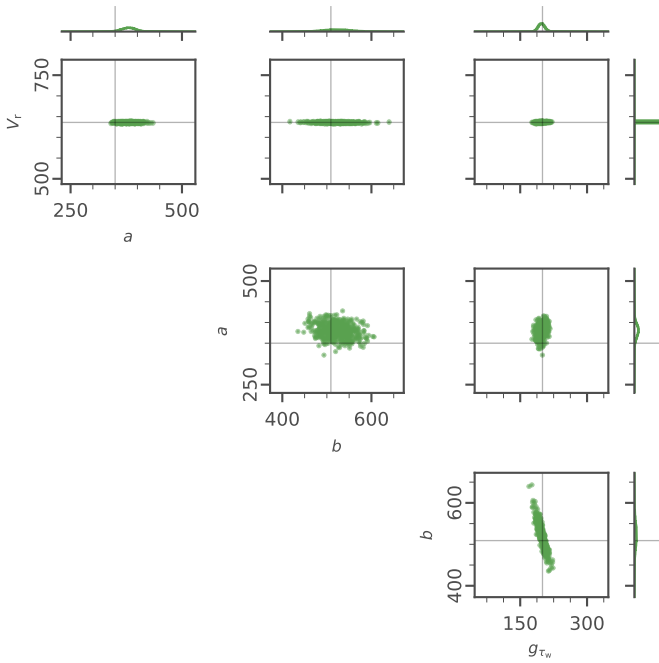


Figure 4. **Samples drawn from the approximated posterior** – One- and two-dimensional marginals of 500 samples drawn from the approximated posterior. The vertical and horizontal lines represent the parameterization of the target trace. Note, uniform priors from 0 to 1022 were chosen for all parameters, i.e. the posterior distribution is restricted to a much smaller region of the parameter space.

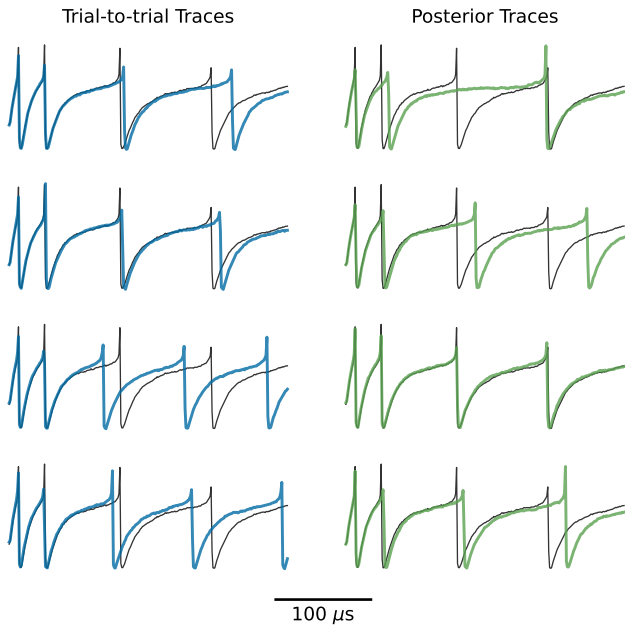


Figure 5. **Example traces for different experiment trials and parameterizations drawn from the approximated posterior** – Black traces represent the chosen target observation. On the left side, the experiment is repeated several times with the same parameterization. Due to temporal fluctuations in the analog components of BrainScaleS-2, the traces do not align exactly. However, the overall behavior matches between all traces. On the right side, we drew four parameterizations from the approximated posterior, fig. 4, and emulated the neuron behavior.

leveraged to infer model parameters for the adaptive exponential integrate-and-fire (AdEx) neuron model emulated on the neuromorphic BrainScaleS-2 (BSS-2) system when utilizing membrane recordings as observations. Despite the presence of temporal noise on the hardware, the algorithm was able to approximate the posterior distribution, thereby enabling adequate emulation of the target trace.

We began by generating a dataset consisting of diverse voltage traces. After initial preprocessing of the data, a convolutional autoencoder was successfully trained, whose encoder was then used to compress the time series data into just 32 features. Subsequently, this lower-dimensional representation of the data was fed into the neural density estimator (NDE) of the SNPE algorithm. To further enhance inference performance, we chose to simultaneously retrain the pretrained encoder alongside the NDE. Our method yielded promising results, as the algorithm was able to identify the correct region within the 4-dimensional parameter space, even in the presence of the trial-to-trial variations inherent to the hardware.

The reconstructions of the autoencoder could have been improved by selecting a larger latent space dimension. However, a balance must be struck between reconstruction accuracy and dimensionality reduction for the SNPE algorithm. As shown in fig. 3, the reconstructions of traces with stronger adaptation are worse than those of other traces. This is due to the low occurrence of adaptation traces in the training set — only a small subset of the chosen parameter space produces such traces. Since our observation was an adaptation trace, this reinforces our decision to simultaneously retrain the encoder with the NDE.

Temporal noise in the analog components leads to the approximation of the posterior being broader, as parameter values that would typically produce a different voltage trace might resemble one that closely matches the initial target trace. Thus, these values are interpreted as if they produce results similar to those of the true parameters. At the same time, the target trace itself could represent a variation of the typical trace at the target parameters. This would explain the slight offset between the peak of the posterior distribution and the true parameter values, as displayed in fig. 4.

For g_{τ_w} and V_r , more narrow marginals could be identified than for the other two parameters, see fig. 4. However, a broader posterior does not necessarily indicate a worse performance of the approximation method, as certain variations in a parameter may not significantly impact the resulting trace. Furthermore, compensation mechanisms between parameters might exist. For instance, such a relationship was particularly evident between the spike-triggered adaptation b and the conductance g_{τ_w} , exhibiting a negative correlation due to the specific circuit design [12].

Finally, taking trial-to-trial variations into account, most of the emulated traces of randomly sampled posterior values closely resemble the original target trace, as shown in fig. 5. Hence, our method utilizing the autoencoder proved effective and eliminated the reliance on handcrafted features for the

dimensionality reduction of the traces.

The future objective of this work is to develop an inference pipeline for membrane voltage recordings from biological neurons to enable precise emulation. However, this requires the accurate inference of more parameters of the BSS-2 system [11]. To achieve this, several optimizations of our method can be explored.

First, extensive testing and hyperparameter searches for the NDE in higher-dimensional parameter spaces are needed to assess the robustness of our current method.

Furthermore, different autoencoder architectures could be explored to improve compression efficiency. The input size of the network could be increased too, allowing it to handle traces emulated for longer durations.

In addition, approaches to address temporal noise could be considered to potentially achieve a more accurate posterior, as this noise also complicates posterior analysis. Building on this, ensembles comprising multiple posteriors from various emulations of the true parameters might counteract overconfident posterior estimates [27].

Finally, the posterior distribution needs to undergo more rigorous testing. A suitable metric for measuring the similarity between different voltage traces must be established, such that systematic posterior-predictive checks can be performed [27]. These would filter out posterior estimates that do not align well with the observation. Moreover, the posterior could be used to explore further correlations between different parameters. Additionally, sensitivity analysis could help identify critical directions in the parameter space where changes in the parameters have a strong impact on the resulting trace [28].

To date, studies have primarily applied the SNPE algorithm to reproduce the behavior of spiking neurons in numerical simulations [6], [8], [9] or of passive neurons on neuromorphic hardware [10]. Thus, this work represents a novel approach and an initial step towards applying the algorithm to reproduce biological neuron behavior on neuromorphic hardware. Fast emulation on accelerated neuromorphic hardware has the potential to explore new questions that are difficult to address by slower numerical simulation techniques [29]. Consequently, the combination of automatic feature extraction with the application of the SNPE algorithm for emulation on neuromorphic hardware could contribute to shaping future methodologies in neuroscience research.

ACKNOWLEDGEMENTS

This research has received funding from the European Union's Horizon 2020 research and innovation programme under grant agreement No. 945539 (Human Brain Project SGA3) and Horizon Europe grant agreement No. 101147319 (EBRAINS 2.0), and the Deutsche Forschungsgemeinschaft (DFG, German Research Foundation) under Germany's Excellence Strategy EX 2181/1-390900948 (the Heidelberg STRUCTURES Excellence Cluster).

AUTHOR CONTRIBUTIONS

We give contributions in the *CRedit* (Contributor Roles Taxonomy) format: **JH**: Investigation, visualization, methodology,

software; **JK**: Conceptualization, methodology, supervision, software, visualization; **EM**: Conceptualization, methodology, supervision, software, resources; **JS**: Conceptualization, methodology, supervision, funding acquisition; **all**: writing — original draft, writing — reviewing & editing.

REFERENCES

- [1] M. C. Vanier *et al.*, “A comparative survey of automated parameter-search methods for compartmental neural models,” *J Comput Neurosci*, vol. 7, no. 2, pp. 149–171, 1999. DOI: 10.1023/a:1008972005316.
- [2] N. W. Gouwens *et al.*, “Systematic generation of biophysically detailed models for diverse cortical neuron types,” *Nature communications*, vol. 9, no. 1, p. 710, 2018. DOI: <https://doi.org/10.1038/s41467-017-02718-3>.
- [3] S. Druckmann *et al.*, “A novel multiple objective optimization framework for constraining conductance-based neuron models by experimental data,” *Front Neurosci*, vol. 1, no. 1, pp. 7–18, Nov. 2007. DOI: 10.3389/neuro.01.1.1.001.2007.
- [4] M. Deistler *et al.*, *Differentiable simulation enables large-scale training of detailed biophysical models of neural dynamics*, 2024. bioRxiv: 2024.08.21.608979.
- [5] K. Cranmer *et al.*, “The frontier of simulation-based inference,” *Proceedings of the National Academy of Sciences*, vol. 117, no. 48, pp. 30 055–30 062, 2020. DOI: 10.1073/pnas.1912789117.
- [6] J.-M. Lueckmann *et al.*, “Flexible statistical inference for mechanistic models of neural dynamics,” in *Advances in Neural Information Processing Systems*, vol. 30, 2017.
- [7] D. Greenberg *et al.*, “Automatic posterior transformation for likelihood-free inference,” in *Proceedings of the 36th International Conference on Machine Learning*, vol. 97, PMLR, 2019, pp. 2404–2414.
- [8] P. J. Gonçalves *et al.*, “Training deep neural density estimators to identify mechanistic models of neural dynamics,” *eLife*, vol. 9, Sep. 2020. DOI: 10.7554/eLife.56261.
- [9] M. Deistler *et al.*, “Truncated proposals for scalable and hassle-free simulation-based inference,” *arXiv preprint*, 2022. DOI: 10.48550/arxiv.2210.04815.
- [10] J. Kaiser *et al.*, “Simulation-based inference for model parameterization on analog neuromorphic hardware,” *Neuromorphic Comput. Eng.*, vol. 3, no. 4, p. 044 006, 2023. DOI: 10.1088/2634-4386/ad046d.
- [11] C. Pehle *et al.*, “The BrainScaleS-2 accelerated neuromorphic system with hybrid plasticity,” *Front. Neurosci.*, vol. 16, 2022. DOI: 10.3389/fnins.2022.795876.
- [12] S. Billaudelle *et al.*, “An accurate and flexible analog emulation of AdEx neuron dynamics in silicon,” in *29th IEEE International Conference on Electronics, Circuits and Systems (ICECS)*, 2022, pp. 1–4. DOI: 10.1109/ICECS202256217.2022.9971058.

- [13] R. Brette *et al.*, “Adaptive exponential integrate-and-fire model as an effective description of neuronal activity,” *J. Neurophysiol.*, vol. 94, pp. 3637–3642, 2005. DOI: 10.1152/jn.00686.2005.
- [14] M. Hock *et al.*, “An analog dynamic memory array for neuromorphic hardware,” in *Circuit Theory and Design (ECCTD), 2013 European Conference on*, Sep. 2013, pp. 1–4. DOI: 10.1109/ECCTD.2013.6662229.
- [15] G. Papamakarios *et al.*, “Fast ε -free inference of simulation models with bayesian conditional density estimation,” in *Advances in Neural Information Processing Systems*, vol. 29, Curran Associates Inc., 2016, pp. 1036–1044.
- [16] G. Papamakarios *et al.*, “Masked autoregressive flow for density estimation,” in *Advances in Neural Information Processing Systems*, vol. 30, 2017.
- [17] G. Papamakarios *et al.*, “Sequential neural likelihood: Fast likelihood-free inference with autoregressive flows,” in *Proceedings of the Twenty-Second International Conference on Artificial Intelligence and Statistics*, ser. Proceedings of Machine Learning Research, vol. 89, PMLR, Apr. 2019, pp. 837–848.
- [18] P. Li *et al.*, “A comprehensive survey on design and application of autoencoder in deep learning,” *Applied Soft Computing*, vol. 138, p. 110176, 2023. DOI: 10.1016/j.asoc.2023.110176.
- [19] O. Yildirim *et al.*, “An efficient compression of ECG signals using deep convolutional autoencoders,” *Cognitive Systems Research*, vol. 52, pp. 198–211, 2018. DOI: 10.1016/j.cogsys.2018.07.004.
- [20] R. Naud *et al.*, “Firing patterns in the adaptive exponential integrate-and-fire model,” *Biological Cybernetics*, vol. 99, no. 4, pp. 335–347, Nov. 2008. DOI: 10.1007/s00422-008-0264-7.
- [21] E. Müller *et al.*, “A scalable approach to modeling on accelerated neuromorphic hardware,” *Front. Neurosci.*, vol. 16, 2022. DOI: 10.3389/fnins.2022.884128.
- [22] A. P. Davison *et al.*, “PyNN: A common interface for neuronal network simulators,” *Front. Neuroinform.*, vol. 2, no. 11, 2009. DOI: 10.3389/neuro.11.011.2008.
- [23] D. P. Kingma *et al.*, “Adam: A method for stochastic optimization,” *International Conference on Learning Representations*, 2014.
- [24] A. Paszke *et al.*, “Pytorch: An imperative style, high-performance deep learning library,” in *Advances in Neural Information Processing Systems 32*, H. Wallach *et al.*, Eds., Curran Associates, Inc., 2019, pp. 8024–8035.
- [25] J.-M. Lueckmann *et al.*, “Benchmarking simulation-based inference,” in *Proceedings of the 24th International Conference on Artificial Intelligence and Statistics (AISTATS)*, vol. 130, PMLR, 2021, pp. 343–351.
- [26] A. Tejero-Cantero *et al.*, “Sbi: A toolkit for simulation-based inference,” *Journal of Open Source Software*, vol. 5, no. 52, p. 2505, 2020. DOI: 10.21105/joss.02505.
- [27] J. Hermans *et al.*, “A crisis in simulation-based inference? beware, your posterior approximations can be unfaithful,” *Transactions on Machine Learning Research*, 2022.
- [28] P. G. Constantine *et al.*, “Active subspace methods in theory and practice: Applications to kriging surfaces,” *SIAM J. Sci. Comput.*, vol. 36, no. 4, A1500–A1524, 2014. DOI: 10.1137/130916138.
- [29] F. Zenke *et al.*, “Limits to high-speed simulations of spiking neural networks using general-purpose computers,” *Front. Neuroinform.*, vol. 8, no. 76, 2014. DOI: 10.3389/fninf.2014.00076.